

**EFFECT OF MOLDS ON CURING IN PDMS FABRICATION AND
DEFORMATION IN PDMS BASED MICROFLUIDIC CHIPS**

by

Rabia Mercimek

A Master Thesis

Submitted in fulfilment of the requirement for the degree of Master

Department of Material Science and Nano Engineering

Sabanci University

Spring, 2023

© Rabia MERCIMEK

All Rights Reserved

To my dear family and friends who are always by my side...

ABSTRACT

EFFECT OF MOLDS ON CURING IN PDMS FABRICATION AND DEFORMATION IN PDMS BASED MICROFLUIDIC CHIPS

Rabia Mercimek

MATERIALS SCIENCE AND NANO ENGINEERING

MSc. THESIS, December, 2023 Thesis

Supervisor: Prof. Dr. Ali Koşar

Keywords: Microfluidics, Lab-on-a-Chip , 3D Printed Molds, Soft Lithography

In this thesis, two different approaches on polydimethylsiloxane(PDMS) curing and deformation in microfluidic chips were discussed. PDMS is the most preferred microfluidic chip raw material since it allows easy and cheap fabrication of microfluidic chips compared to other production methods. Biocompatibility, flexibility and easy fabrication of microfluidic chips make PDMS popular material, especially for biotechnological applications such as organ-a-chip devices. Recently, 3D printing has become a popular alternative method in PDMS mold fabrication because it is easy and practical. A wide variety of materials has been used in 3D printing, and it was observed that these materials affect the PDMS curing. The first part of this study examines the effect of molds with the same dimensions, which were fabricated using four different materials, on PDMS curing. The findings indicate that the choice of mold material affects both the curing kinetics of PDMS and consequently, the mechanical properties of the material. However, this influence is not substantial in the overall efficiency of curing at the selected temperatures and curing duration.

PDMS based microfluidic chips deform under the influence of the liquid flowing through microfluidic channels especially near the channel inlet where the pressure is the highest. This change is due to the elasticity of PDMS. In the second part of the thesis, the deformations in microfluidic chips with different dimensions and curing patterns were analyzed. The findings indicate that at low flow rates, the deformation ratio of microchannels with identical dimensions is notably influenced by elasticity. However, as the flow rate increases, the impact of elasticity diminishes.

ÖZET

FARKLI KALIPLARIN PDMS KÜRLENMESİ ÜZERİNDEKİ ETKİSİ VE PDMS MİKROAKIŞKAN ÇİP DEFORMASYONU

Rabia MERCİMEK

MALZEME BİLİMİ VE NANOMÜHENDİSLİK

YÜKSEK LİSANS TEZİ, Aralık 2023

Danışman: Prof. Dr. Ali Koşar

Anahtar Kelimeler: Mikroakışkanlar, Lab-on-a-Chip, 3 Boyutlu Yazıcı, Yumuşak Litografi

Bu tezde mikroakışkan sistemleri temelli iki farklı çalışma ele alınmaktadır. PDMS, diğer üretim yöntemlerine kıyasla daha kolay ve ucuz olması nedeniyle popüler mikroakışkan çip hammaddesidir. Biyouyumlu, esnek ve kolay şekillendirilebilir olması PDMS'yi özellikle organ-çip gibi biyoteknolojik uygulamalar için en kullanışlı malzeme haline getirmektedir. Literatürde PDMS mikro cihaz üretiminin optimizasyonunda kürlenme oranı, pişirme süresi ve karıştırma oranının etkileri üzerine birçok çalışma bulunmaktadır. Son zamanlarda 3D yazıcılar kolay ve pratik olmaları nedeniyle PDMS kalıp üretiminde popüler bir alternatif yöntem haline gelmiştir. 3D yazıcı üretiminde çok çeşitli malzemeler kullanılmaktadır ve PDMS kürlenmesinde kullanılan bu malzemelerin farklı ısı transfer katsayıları nedeniyle kürlenmeyi etkilediği gözlemlenmiştir. Bu çalışmanın ilk bölümünde 4 farklı malzeme ile imal edilen aynı boyutlardaki kalıpların PDMS kürlenmesine etkisi incelenmiştir. Bulgular, kalıp malzemesi seçiminin hem PDMS'nin kürlenme kinetiğini hem de sonuç olarak malzemenin mekanik özelliklerini etkilediğini göstermektedir. Ancak bu etki, seçilen sıcaklıklarda ve kürlenme süresinde kürlenmenin genel verimliliği üzerinde etkili değildir.

PDMS yumuşak ve esnek özelliklere sahip bir malzemedir, bu özellikleri de onu birçok uygulama için uygun hale getirir. Ancak farklı koşullar altında kürlenmiş PDMS farklı esneklik özellikleri gösterebilmektedir. PDMS, kanallardaki akışın uyguladığı basınç etkisi altında esner ve özellikle basıncın en yüksek olduğu kanal girişi esneyerek şekil değiştirir. PDMS'nin esnekliğinden kaynaklanan bu değişim deformasyon olarak adlandırılır. Çalışmanın ikinci bölümünde farklı boyutlara ve kürlenme şekillerine sahip mikroakışkan çiplerin deformasyonları analiz edilmiş ve karşılaştırılmıştır. Çalışmanın sonuçlarına göre, düşük akış hızlarında, aynı boyutlara sahip mikrokanalların deformasyon oranının elastikiyetten önemli ölçüde etkilendiğini göstermektedir. Bununla birlikte, akış hızı arttıkça, elastikiyetin etkisi azalır ve daha yüksek akış hızlarında vurgulanır.

ACKNOWLEDGEMENTS

I would like to emphasize my sincere appreciation to everyone who supported me during this MSc thesis process. I would also like to pay sincere gratitude to all faculty members and staff of Sabancı University especially my advisor Prof. Dr. Ali Koşar, Dr. Morteza Ghorbani for imparting the best of their knowledge to me that made me able to achieve my master studies. I also extend my thanks to Professor Dr. Timm Krueger from the University of Edinburgh, and to Fatemehsadat Mirghaderi, for their invaluable support in my studies. Furthermore, I am thankful to my teammates İsmail Bütün, Ünal Akar, Beyzanur Özogul, Farzad Talabazar, Erçil Toyran, Zülal Müganlı and all the Kosarlab team. I am grateful to my family members, my mom Ayşe Mercimek, my sisters Nur Sima Mercimek, Gülsüm Mercimek, my brother Ömer Faruk Mercimek, my friends Gökmen Tamer, Gülşen Zal, Zobia Batool, Seba Nur Alhasan, Serra Ersoy, Sümeyye Narin, Gülce Güralp, Gülnur Şener, Aybükenur Özer, Ayça Aydurmuş and Ravzanur Yazıcıoğlu for their support, and for providing me with unforgettable memories that will make my master's program more enjoyable. I feel fortunate to have had the opportunity to complete this MSc thesis with your support successfully.

Finally, I thank the Tubitak 1004 Project NANOSIS for the scholarship and research funding.

TABLE OF CONTENT

ABSTRACT	iv
ÖZET	v
TABLE OF CONTENT	vii
LIST OF FIGURES	ix
LIST OF ABBREVIATIONS	x
CHAPTER 1. INTRODUCTION	1
1.1 Microfluidic Technologies	1
1.2 Properties of PDMS	1
1.3 Polydimethylsiloxane (PDMS) in Microfluidic Systems	2
1.4 Elasticity and Measurement Methods	3
1.5 Deformation of PDMS Based Microfluidic Chips	4
1.6 Motivation	5
1.7 Objectives	6
CHAPTER 2. EFFECT OF MOLDS IN PDMS FABRICATION	7
2.1 Materials and Methods	7
2.1.1 Materials	7
2.1.2 Mold Design and Fabrication	7
2.1.3 Experimental Setup	8
2.1.4 PDMS Curing	8
2.1.5 Characterizations	9
2.2 Results and Discussion	12
2.2.1 2.2.1 Heat Transfer	12
2.2.2 Elasticity Measurements	13
2.2.3 Soxhlet Curing Analysis	14
2.2.4 Thermogravimetric Analysis (TGA) Results	14
2.2.5 FTIR Analysis Results	15
2.2.6 Discussion	16
2.3 Conclusion	17
CHAPTER 3. DEFORMATION IN PDMS BASED MICROFLUIDIC CHIPS 18	
3.1 Materials and Methods	18

3.1.1	Materials	18
3.1.2	Instruments	18
3.1.3	Microfluidic Device Design	18
3.1.4	PDMS Microchannel Fabrication	19
3.1.5	Visualization in Microchannel	19
3.1.6	Image Processing	20
3.2	Result and Discussion	21
3.2.1	Calculations of Flow Parameters	21
3.2.2	Deformation Measurements	25
3.3	Conclusion.....	29
CHAPTER 4.....		30
CHAPTER 5. REFERENCES.....		31

LIST OF FIGURES

Figure 1: Polydimethylsiloxane Sylgard® 184 chemical structure [4].....	2
Figure 2: Deformation of PDMS channels a) cross section of channel, b) side view of channel, deformation with pressure differences [19].	5
Figure 3: Mold Design	7
Figure 4: Experimental setup; A) Heat transfer analysis of between PDMS and molds, B) PDMS preparation.....	8
Figure 5: Soxhlet analysis setup.....	11
Figure 6: Temperature profile time, during PDMS curing.	12
Figure 7: Elasticity of PDMS samples cured in different molds, of different times and temperatures A) at 55°C, B) at 65°C and C) at 75°C.	13
Figure 8: Soxhlet analysis results at curing times A) 2 hours B) 12 hours	14
Figure 9: TGA analysis of PDMS samples	15
Figure 10: FTIR results of PDMS samples.	16
Figure 11: Microfluidic device designs and parameters.....	18
Figure 12: Experimental setup of deformation experiments under confocal microscope.	20
Figure 13: Confocal Images of Microfluidic Device	21
Figure 14: Part of channel with distance distribution for image analysis.	21
Figure 15: Nusselt number and friction factors for laminar flows [17,18].	23
Figure 16: Deformation of PDMS microchannel with distance of channel	25
Figure 17: Deformation of microchannels with 10 mm length, flow rate	26
Figure 18: Deformation of microchannels with 10 mm length in term of pressure drop.	26
Figure 19: Deformation of microchannels with 20 mm length, as a function flow rate.....	27
Figure 20: Deformation of microchannels with 20 mm length, as a function of pressure drop.....	28
Figure 21: Deformation of microchannels with different elasticity and dimensions of 10 mm length 100 um width 100 um height.	29

LIST OF ABBREVIATIONS

PDMS	:	Polydimethylsiloxane
PLA	:	Polylactic Acid
PET	:	Polyethylene terephthalate
Al	:	Aluminum
CNC	:	Computer Numerical Control
AFM	:	Atomic Force Microscopy
TGA	:	Thermogravimetric Analysis
SEM	:	Scanning Electron Microscopy
UV-VIS	:	UV-Visible Spectrophotomete

CHAPTER 1. INTRODUCTION

1.1 Microfluidic Technologies

Microfluidic technologies involve systems that mimic large-scale systems and provide new alternatives with microfluidic devices designed and fabricated in micro dimensions. Microfluidic technology started in the 1990s with the emergence of cleanroom technologies that enable micro and nano-scale production [1]. These systems occupy less space due to their small size, and their fabrication is often less costly than other systems. By manipulating the physics of flow, microfluidic systems can be designed for applications such as separation, mixing, purification and focusing. In addition to these applications, microfluidic systems are also designed for applications such as energy harvesting [2] and wastewater treatment [3]. These systems, which are widely preferred in biomedical applications, provide shorter and more efficient results in diagnosis and treatment than other methods.

Microfluidic technologies are also known as lab-on-a-chip technologies. Many different methods and materials are used to fabricate microfluidic chips. Glass, metal, semiconductors such as silicon, ceramic, paper and polymer are major materials used in the production of these devices. Lithography, material removal methods, material additive methods are used in their fabrication. Microfluidic devices are fabricated using these materials or systems that combine these materials in accordance with the characteristics and requirements of the system depending on the application.

1.2 Properties of PDMS

In the field of microfluidics, polydimethylsiloxane (PDMS), has become popular. Although polymers are utilized in many areas of engineering, silicones, PDMS in particular, have drawn attention due to its remarkable properties. Polydimethylsiloxane is one of the most preferred materials in lab-on-chip applications due to its ability to easily mimic biological systems due to transparency, biocompatibility, elasticity and machinability [4]. The ease of fabrication and being low cost highlight its broad availability. It is a material that can be easily obtained for a range of scientific and engineering purposes. In addition, PDMS is transparent, which makes it easy to control and visualize the system. Dow Corning's Sylgard 184 is a product that has been

extensively used in microfluidic applications [5]. This product has the two-part form of PDMS, which consists of a crosslinker and a base polymer and enables customization of its physicomechanical characteristics (Figure 1).

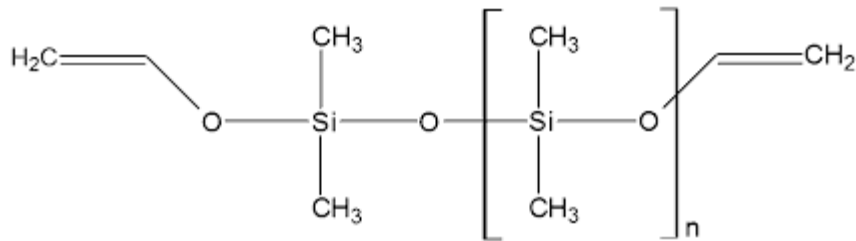


Figure 1: Polydimethylsiloxane Sylgard® 184 chemical structure [6]

The hyperelasticity of PDMS to experience reversible deformation and regain its normal shape upon the removal of applied force is what makes it so significant. This special mechanical characteristic is important for many applications, especially in soft lithography and microfluidics. One important feature that makes PDMS applicable in many domains, especially in microfabrication and microfluidics, is thus its elasticity. The success of numerous technologies and developments is attributed to its reversible deformation and robustness. The flexibility of PDMS is useful for biological and biomedical applications, including organ-on-a-chip systems and cell culture platforms. By simulating the mechanical characteristics of soft tissues, the material can offer cell growth and tissue formation in a more physiologically realistic environment.

1.3 Polydimethylsiloxane (PDMS) in Microfluidic Systems

It is commonly known that cell culture plays a crucial role in our understanding of cell behavior, mutations throughout time, responses to external stimuli, and interactions between cells [7,8]. Although conventional in vitro techniques are extensively standardized, they are costly and require less expensive and labor-intensive substitutes. Microfluidic technology has surfaced as a promising alternative that enables the replacement of traditional petri dishes and flasks with microscale cell culture systems.

For several reasons, microfluidics has become more popular for. This method uses less reagent and sample volume, which reduces expenses. Additionally, it offers improved control over the cellular environment, which is essential for modifying the surroundings

in order to affect cellular processes. Prior research, including the study by Kim et al. [9] used microfluidic chips to stimulate brain stem cell differentiation and proliferation which exhibited concentration-dependent responses akin to those seen in conventional cultures. In a different study by (Jean et al.) [10], human mesenchymal cells (MSCs) were cultured in 96 individually addressable culture chambers using a microfluidic system to regulate their proliferation and promote their differentiation. Given the circumstances, microfluidic cell culture techniques provide affordable, regulated, and tailorable platforms for further cell biology research.

Separation plays a key role in both preparative and analytical applications which allows for the purification of samples and the study of separated objects [10]. Size-based sorting in microfluidics has various applications in industrial production, food and chemical industries, environmental assessment, and research.

The ability to separate cells based on their physical properties is emphasized, which highlights its importance in health, research, and industry [11]. Diseases often alter the physical properties of cells which makes cell sorting a valuable diagnostic tool. In the study of (Islam and Chen) [11], for example, passive sorting of tumor cells from engineered blood cells was considered based on size differences.

Micromixers, another important application area of microfluidic technologies, provide mixing of flows and streams precisely and efficiently. Unlike macroscale fluidic devices, where the mixing of fluids is usually based on diffusion effects, mixing in microfluidic devices is usually achieved by external turbulence in microchannels and/or by specialized microstructures with micro-level dimensions to achieve a larger surface-to-volume ratio and improve heat and mass transfer efficiency [12, 13].

1.4 Elasticity and Measurement Methods

Elasticity is the ability of a material to deform under stress. Elasticity characterization methods play an important role in understanding the mechanical properties of materials and provide information about their response under applied stress. Tensile testing, a widely used technique, involves subjecting materials to axial stress until failure while simultaneously measuring stress and strain [14]. This method is particularly applicable to deformable materials such as metals, polymers and elastomers. Young's modulus, a key indicator of material stiffness, is derived from the first linear segment of the stress-strain curve and provides a quantitative measure of a material's ability to resist

deformation. The initial linear section of the stress-strain curve is used to compute the Young's modulus (E) in tensile testing. It represents the relationship between strain (ϵ) and stress (σ) in the region of elastic deformation. It can be stated mathematically as $E = \Delta\sigma / \Delta\epsilon$ where $\Delta\sigma$ represents the change in stress and $\Delta\epsilon$ represents the change in strain.

Along with tensile testing, compression test serves as a similar method for deformable materials and focuses on compression forces and providing data on the behavior of the material under compression. The force-depth connection during indentation is measured via nanoindentation. Using the Oliver-Pharr approach, one may determine the Young's modulus (E), which can be stated as: $E = (1/S)(dP/dh)$ where S is a geometric factor, dP/dh is the unloading curve's slope, P is the pressure applied on material and h is the indentation depth.

Nanoindentation using a sharp indentation at the nanoscale is versatile, suitable for both deformable and non-deformable materials, and offers precise measurements of Young's modulus based on indentation depth and force data [15].

Dynamic Mechanical Analysis (DMA) extends the scope of elasticity characterization by evaluating mechanical properties as functions of temperature, time or frequency. This method is well suited for deformable materials such as polymers and composites with Young's modulus derived from the storage modulus. The storage modulus and the Young's modulus of a linear viscoelastic material can be related to each other using the expression, $E = 2(1 + \nu)E'$ where ν is the Poisson's ratio.

Atomic Force Microscopy (AFM) complements these techniques by providing a means to map surface topography and determine local elastic properties, particularly advantageous for soft materials and biological samples [16]. The force applied to the sample affects the AFM cantilever's deflection. Young's modulus values are frequently obtained from cantilever deflection using Hertzian contact mechanics. In this thesis, elasticity characterization of the PDMS samples were carried out by using this method.

1.5 Deformation of PDMS Based Microfluidic Chips

Elastic materials are materials that have the ability to deform under stress and then return to their original state [17]. PDMS, an elastic material, also changes shape under stress. PDMS based microfluidic devices are deformed due to pressure exerted by the flow through the microchannels. This deformation is an advantage in biological applications

as PDMS is flexible like the membranes of cells and helps cell proliferation and ensures its compatibility with cells, however, this deformation rate needs to be optimized in order to successfully control the systems and operation.

In the literature, the deformation of PDMS microchannels an example study by (Gervais et al.) [18] examined the elastic deformation of PDMS microchannels under varying flow rates and investigated its effect on laminar flow profiles and pressure distribution within the channels (Figure 2). The compliance of PDMS, a characteristic feature of soft lithography, sets it apart from traditional micromachining materials. This thesis emphasizes on the importance of considering deformation, particularly in channels with low aspect ratios. Confocal microscopy images taken under different flow conditions are presented. As a result, a comprehensive analysis was performed to assess numeric effects.

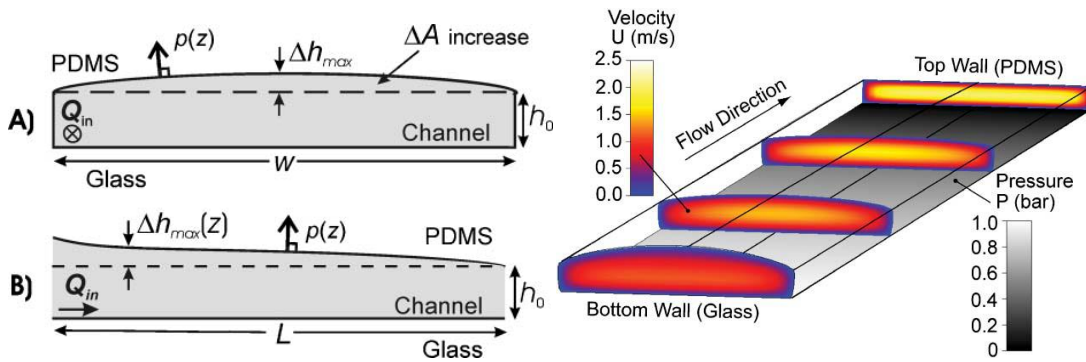


Figure 2: Deformation of PDMS channels a) cross section of channel, b) side view of channel, deformation with pressure differences [18].

1.6 Motivation

PDMS is a material of choice for the fabrication of microfluidic devices due to its biocompatibility, flexibility and transparency. Although a significant amount of research effort has been made on optimizing the fabrication of PDMS microfluidic offers new insights and information are included in this thesis devices, by considering variables such as cure rate, baking time, mixing ratio, the effect of different mold usage on PDMS curing.

While there are many studies on PDMS based microfluidic chips, few studies focus on the deformation of these chips under flow conditions. In the second part, deformation analysis and comparison of PDMS microchannels with different dimensions and

elasticity are presented to address the lack of experimental studies on PDMS microfluidic chips related for this topic.

1.7 Objectives

This thesis has two main objectives. The first aim is to assess the effects of mold material selection on the overall optimization of PDMS microfluidic device fabrication.

In the second part, the focus is on the analysis and comparison of deformation in PDMS microfluidic chips with different dimensions and curing patterns. The aim is to unravel the complex relationship between the elastic properties of PDMS and resulting deformation under flow conditions. In particular, this thesis explains how PDMS exhibits deformation under the influence of fluid flow through microchannels by highlighting variations in dimensions and curing patterns. By achieving these goals, the thesis will offer valuable results for optimizing microfluidic devices applications such as organ-on-chip devices.

CHAPTER 2. EFFECT OF MOLDS IN PDMS FABRICATION

2.1 Materials and Methods

2.1.1 Materials

In the thesis, PDMS (SYLGARD™ 186 Silicone Elastomer Kit) was used as the base material, BASF Ultrafuse PLA Filament - Apricot Skin 2.85 mm, BASF Ultrafuse Pet Filament - Transparent 2.85 mm, Formlabs Greyscale Resin and Aluminum 7075 were used as PDMS pouring mold materials. A K-type TP-01 thermocouple was used to determine the time to reach the desired temperature during heat transfer experiments.

2.1.2 Mold Design and Fabrication

The effect of using different molds on PDMS curing was investigated. For this purpose, molds with a depth of 1.92 mm, a width of 10.4 mm and a length of 16 mm were designed using the SolidWorks software (Figure 3). Four different materials were used in the production of the mold; Al, PLA, PET and Resin. The materials were selected as Resin, PLA, PET, which are frequently used in the literature in 3D printing applications, as well as Al.

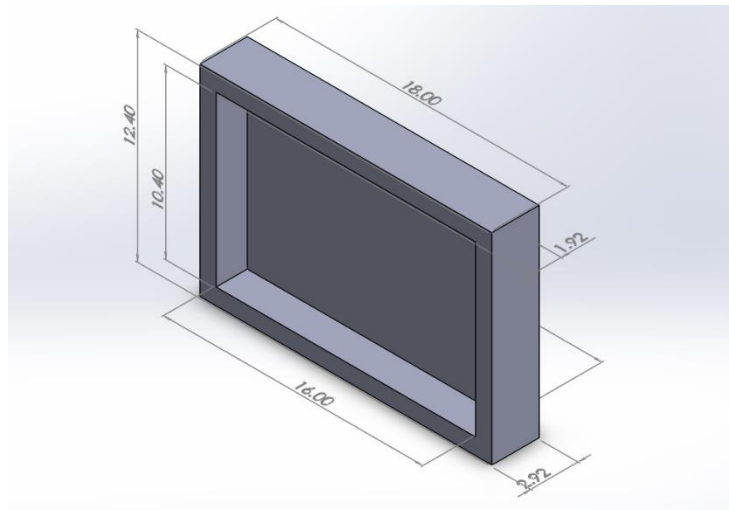


Figure 3: Mold Design

Four distinct mold materials were then chosen to develop molds made of various materials. PET molds were produced using Anycubic 3D printers, which has strong chemical resistance. PLA was used as the mold material, and 3D printers of the Ultimaker-3 were used to create easily separated and eco-friendly molds. Resin molds

were created using Formlabs 3D printers, which provide high-resolution accuracy. Using Computer Numerical Control (CNC) and lathe equipment, aluminum molds with their exceptional heat conductivity and durability were produced.

2.1.3 Experimental Setup

Experiments were performed to examine heat transfer properties of different molds (Figure 4). A K-type thermocouple was positioned on each mold in order to collect temperature data. The molds were then concurrently put into an oven that had been preheated to the temperature of 75°C. This starting point was selected as a standard PDMS curing environment.

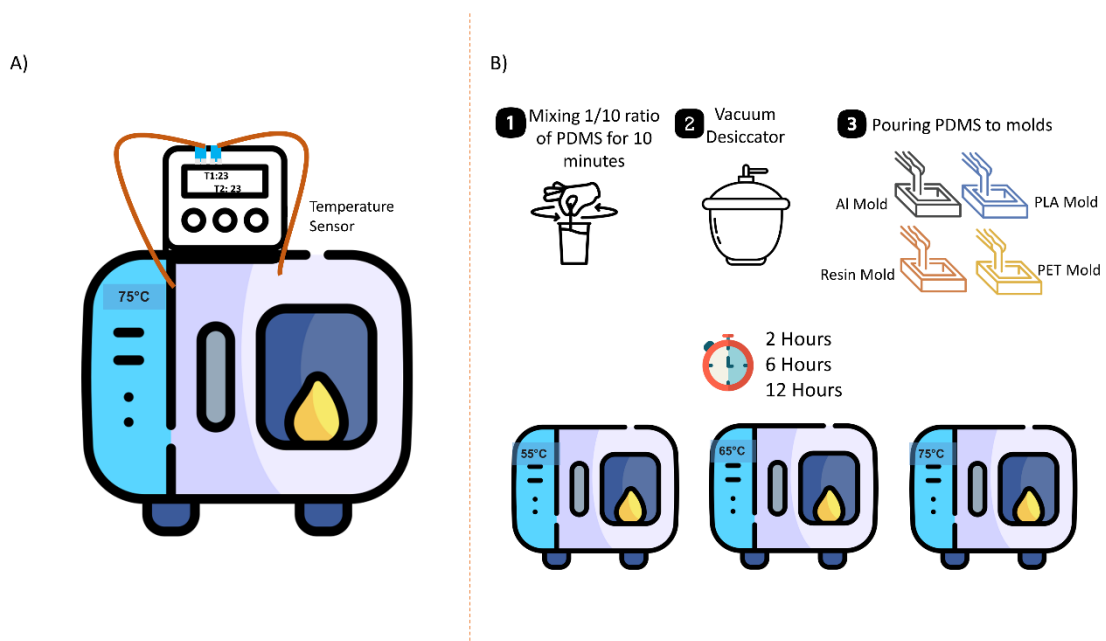


Figure 4: Experimental setup; A) Heat transfer analysis, B) PDMS preparation

2.1.4 PDMS Curing

In order to fabricate PDMS chips, a 10:1 (by weight) mixture that included PDMS elastomer base and curing agent was prepared, mixed for ten minutes, and then put to vacuum desiccator to eliminate any air bubbles before being poured into molds. The mixture was heated to 55°C, 65°C, and 75°C in an oven, respectively, to cure it. Furthermore, at these various temperatures, three distinct curing times—two hours, six hours, and twelve hours—were selected. We then looked at the mechanical and thermal results.

2.1.5 Characterizations

Mechanical, thermal and structural analyses were performed to compare PDMS samples cured using different molds at different temperatures. First, the elasticity forces of 36 samples were analyzed by AFM, and young modulus values were calculated. Curing rates of PDMS samples were determined by the Soxhlet analysis. TGA analysis was performed to compare the thermal durability. FTIR was also performed.

2.1.5.1 Atomic Force Microscopy Elasticity Characterization

Young modulus is the linear relationship between unit strain and normal stress in elastic deformation. It is sometimes referred as the elasticity or modulus of elasticity. This elasticity modulus could be measured using a variety of tools. To evaluate stress-strain, a tensile test is usually performed. The Young modulus coefficient is then computed using the test data. In this thesis, the elasticity coefficient was determined using the Atomic Force Microscope (AFM) method because of the small dimension of the fabricated PDMS sample and the requirement for more sensitive measurements.

To compute the Young's modulus of elasticity values of PDMS samples tapping mode in AFM was used. In this mode, the cantilever taps and retracts softly, applying and removing a little amount of pressure on the sample. This motion is compared to the action of a spring that is flexible, and at the point of contact, energy is transformed.

The energy stored in the sample ($\Delta E_{p,c}$) at each cantilever contact is proportional to its spring constant (k_c):

$$\Delta E_{p,c} = 1/2 k_c (A_0^2 - A^2),$$

where A_0 and A are the free and restricted amplitudes of the cantilever, respectively.

The spring constant (k_c) of the sample is related to the energy stored in it ($\Delta E_{p,c}$) at each cantilever contact:

$$\Delta E_{p,c} = 1/2 k_c (h_0 - h)^2,$$

In the case of AFM, when the tip may be assumed as a sphere of radius R with a substantially larger Young's modulus than the flat sample, the Hertzian model leads to the following formula:

$$(h_0 - h)^3 = [9 (1-\nu)^2 / 16 RE]^2 F^2,$$

where F is the loading force, E is the Young's modulus, w_s is the width measured at half-maximum and ν is the Poisson ratio. The following formula can be used to get the Young's modulus of elasticity, assuming a normal Poisson ratio of 1/3:

$$E = F/w_s h^{1/2} (h_0-h)^{-3/2}.$$

2.1.5.2 Soxhlet Analysis

PDMS samples cured in different molds, were characterized of different temperatures and durations by soxhlet extraction (Figure 5). A soluble substance can be extracted from a solid matrix in a lab setting using the soxhlet extraction procedure, which usually requires the use of a solvent. Soxhlet extraction is a technique frequently used to extract and analyze materials, including additives or byproducts. In the study by Jessamine [19], 38 different solvents were tested for PDMS, and chloroform was selected as one of the fifth best solvents, so that chloroform was used to dissolve uncured PDMS. Each specimen, approximately 0.3-0.4g, was extracted with chloroform for 24 hours and dried at 70°C oven for 24 hours. After drying, the samples were weighed one by one, and curing percentages were determined as:

$$\% \text{ Curing} = (m_2/m_1)100$$

where m_1 is the mass of PDMS cured before extraction, and m_2 is the mass of cured PDMS after extraction.



Figure 5: Soxhlet analysis setup

2.1.5.3 Thermogravimetric Analysis

Thermogravimetric analysis (TGA) is used to examine the heat stability and decomposition behavior of materials, particularly polymers. Using a controlled temperature program in inert atmosphere, TGA measures a sample's weight change as a function of temperature (or time). The thermal stability and degradation characteristics of the cured polydimethylsiloxanes (PDMS) were systematically examined utilizing TGA (Shimadzu DTG-60H), operating at temperatures reaching 1000°C with a heating rate of 10°C per minute, and conducted under a controlled nitrogen atmosphere.

2.1.5.4 Fourier Transform Infrared Spectroscopy Analysis

Fourier Transform Infrared Spectroscopy analysis was performed with FTIR (Thermo Scientific/ IS10) device by taking 64 scans in the range of 400-4000 cm^{-1} for all cured materials.

2.2 Results and Discussion

2.2.1 Heat Transfer

To ensure sample integrity and reliability, the heat transfer experiments were conducted in triplicate at 75 °C for 30 minutes. The average findings are displayed in Figure 6. given its superior heat conductivity, the aluminum mold warmed up and reached oven temperature more quickly than the other molds. It is interesting to note that after reaching thermal equilibrium with the oven all of the molds attained the correct temperature within around 15 minutes. The temperature rise is quicker for Al mold as expected.

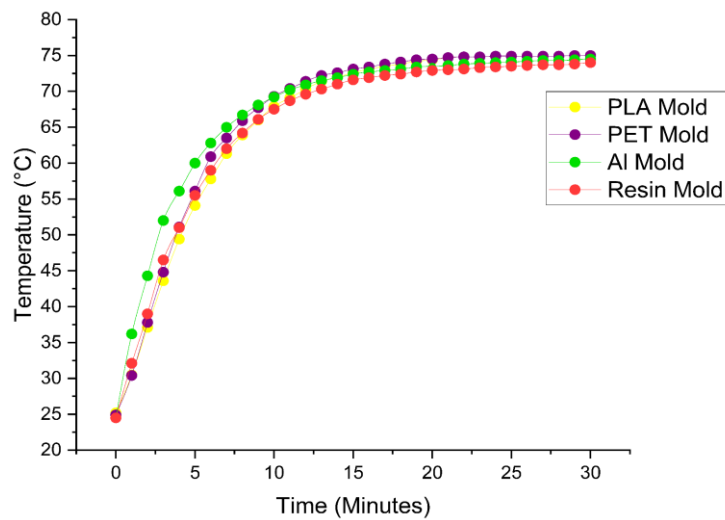


Figure 6: Temperature profile time, during PDMS curing.

2.2.2 Elasticity Measurements

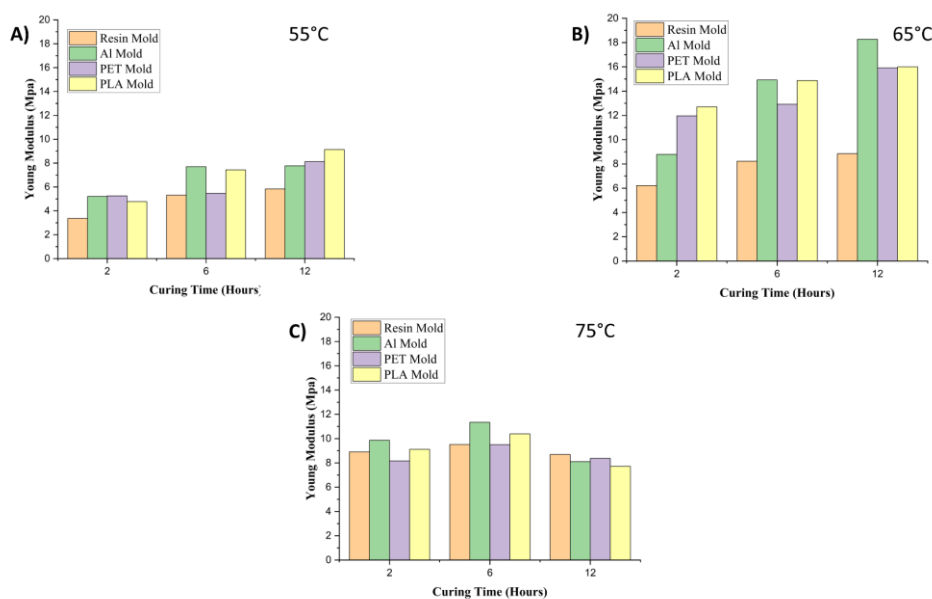


Figure 7: Elasticity of PDMS samples cured in different molds, of different times and temperatures A) at 55°C, B) at 65°C and C) at 75°C.

The results of Young's modulus of elasticity are displayed in Figure 7. The Young's modulus of elasticity values of PDMS cured at the lowest temperature (55 degrees Celsius) are lower than those cured at higher temperatures, as expected due to the reduced curing efficiency. However, the Young's modulus of samples cured at 65 degrees Celsius unexpectedly surpass those cured at 75 degrees Celsius. This observation may indicate that there is no directly proportional relationship between the curing temperature and Young's modulus.

Interestingly, our study reveal that while the different mold materials do not significantly impact the overall curing, their inherent thermal properties influence the PDMS curing reaction kinetics. This implies that rapid or slow curing can potentially affect the mechanical properties of the final PDMS product.

2.2.3 Soxhlet Curing Analysis

The results of Soxhlet curing analysis are presented in Figure. 5. As can be seen in Fig. 8, the type of mold used in the fabrication process has a negligible effect on the overall curing efficiency of PDMS. Notably, only the samples cured at a lower temperature (55°C) for a shorter duration (2 hours) exhibit a significantly lower degree of crosslinking compared to all other samples. This suggests that the curing temperature and time have a more pronounced effect on the crosslinking process than the specific mold type.

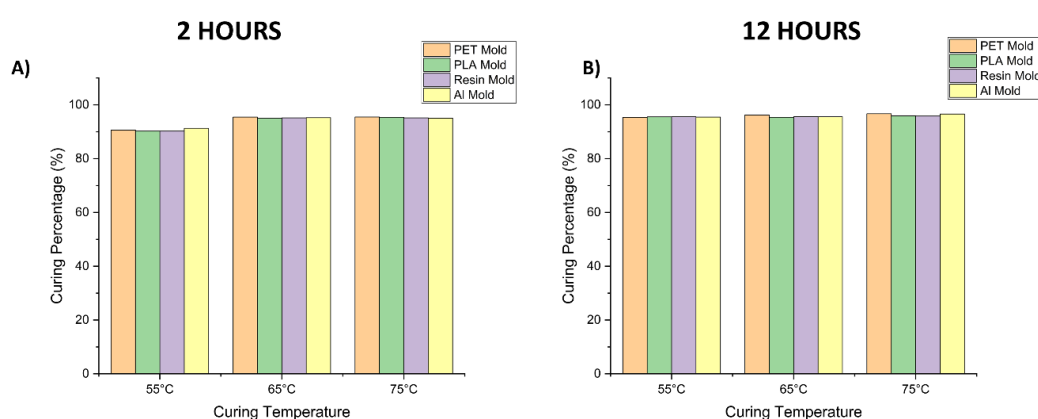


Figure 8: Soxhlet analysis results at curing times A) 2 hours B) 12 hours

2.2.4 Thermogravimetric Analysis (TGA) Results

TGA analysis was performed for different molds for 2 hours. The results of TGA analysis are shown in Figure 9. The starting temperature of degradation is around 205°C. As a result of the Soxhlet analysis, although the curing percentages are almost the same at 55°C for 2 hours, when the mass loss is examined in TGA, the mass loss is found to be less when using aluminum molds. While the mass loss of PDMS is 38% when an Al mold, the mass loss is 42% for PDMS cured in PLA or Resin and 45% for PDMS cured in PET. The thermal conductivity and mass loss of PLA, Resin, and PET molds are close to each other for the highest temperature. The thermal conductivity of the aluminum mold is considerably higher than the other molds, and this results in less mass loss than the others, since a more homogeneous curing can be obtained when using this mold. The PLA, Resin, and PET molds, with smaller thermal conductivities cannot have a

homogeneous curing, and this can be cause a difference in the TGA result compared to Al mold.

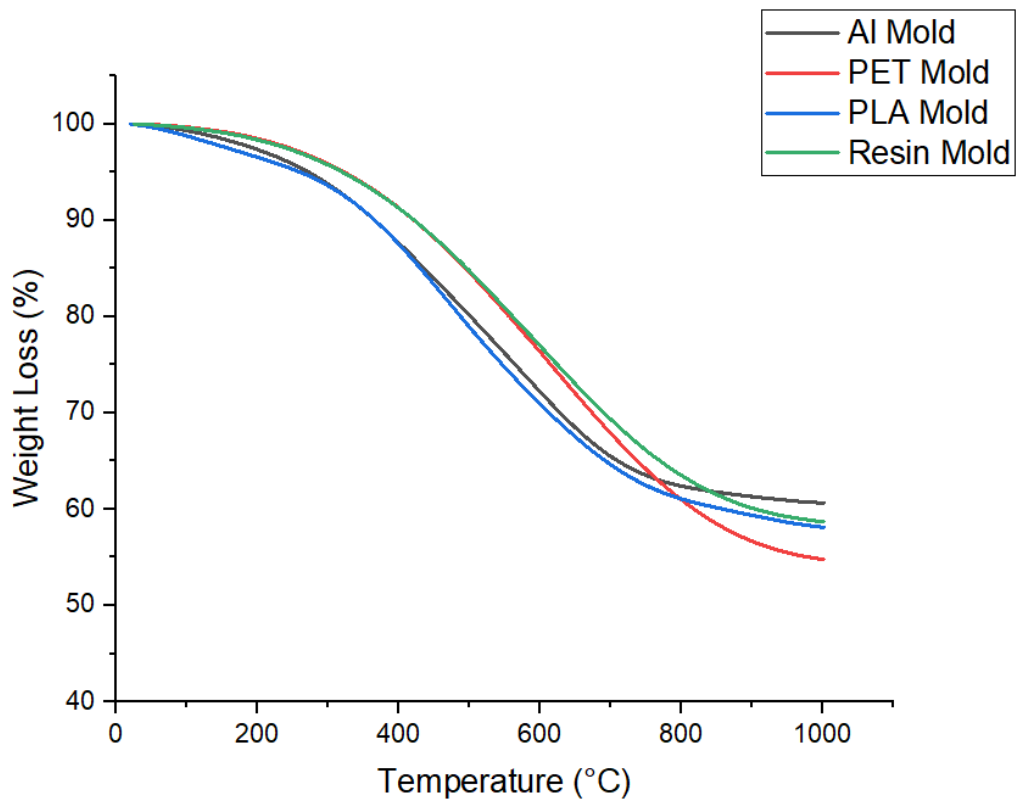


Figure 9: TGA analysis of PDMS samples

2.2.5 FTIR Analysis Results

Figure 10 displays the FT-IR spectrum of the cured PDMS samples. As can be seen, there is no change in the peaks as expected. Because all the materials are the same, there is no change in functional groups during curing in different molds.

The asymmetric stretching of CH_3 in the Si-CH_3 bond is observed around 2960 cm^{-1} wavelength. There is bending motion of C-H molecules in methyl groups around 1410 cm^{-1} . At 1260 cm^{-1} , symmetric deformation motions of CH_3 in the Si-CH_3 bond can be observed. Si-O-Si bonding is observed around a wavelength of $1000\text{-}1050\text{ cm}^{-1}$. The wavelength of $755\text{-}790\text{ cm}^{-1}$ indicates the rocking of Si-C in the Si-CH_3 bond.

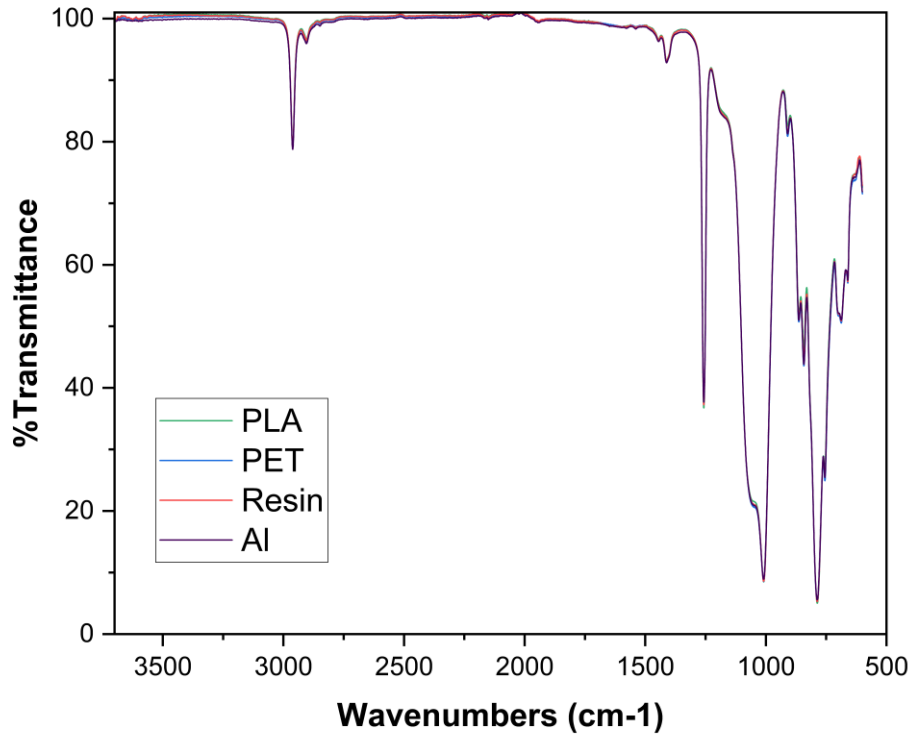


Figure 10: FTIR results of PDMS samples.

2.2.6 Discussion

According to findings in this section, curing at low temperature is easier with PLA and PET molds to control the elasticity of the PDMS based microfluidic chips for Lab-on-a-Chip applications. However, these 2 materials are not capable of withstanding high temperatures. On the other hand, the utilization of a resin mold introduces challenges depending upon the specific resin employed, as chemical reactions might occur. This issue is elucidated in the investigation conducted by (Bazaz et al.) [20], wherein it was demonstrated that the use of DPL resin was not conducive to the curing of PDMS. To address this concern, potential remedies include altering the resin type or implementing post-3D printing treatments on the resin mold. It is noteworthy to underscore that microscale fabrication of aluminum (Al) mold based devices is inherently more intricate and cost-intensive when compared with 3D printing methodologies. However, the incorporation of aluminum mold in this study is justified by its exceptional heat conductivity properties. As the mold size decreases, the surface area directly exposed to heat from the oven to the PDMS mixture decreases which emphasizes on the significance of mold wall thickness and material properties. In smaller dimensions, the heat dissipated

into the mold during curing might result in non-uniform distribution due to the modest thermophysical properties of the mold, influencing accordingly the mechanical properties of PDMS. On the other hand, in larger dimensions, where the surface area is large, the material properties of the mold could be disregarded.

2.3 Conclusion

In order to better comprehend how different mold materials affect PDMS curing properties for Lab-on-a-Chip applications, this section investigated the effects of mold material on curing properties. According to the results, the type of mold material has an impact on the PDMS curing kinetics and in turn on the mechanical properties of the material, but not a significant impact on the overall curing efficiency for chosen temperatures and curing time. The results show that the curing temperature and duration are the main variables affecting the Young's modulus of PDMS. A more crosslinked PDMS structure is promoted by higher temperatures and longer times, which raises the Young's modulus of elasticity.

CHAPTER 3. DEFORMATION IN PDMS BASED MICROFLUIDIC CHIPS

3.1 Materials and Methods

3.1.1 Materials

PDMS (SYLGARD™ 186 Silicone Elastomer Kit) was used. In addition, DI water, Rhodamine B powder for fluorescence (Sigma Aldrich, λ_{ex} 553 nm; λ_{em} 627 nm in methanol), one side polished 4 inch Silicon wafer (University wafer) for producing SU-8 mold, negative photoresist (Microresist Technology) during coating SU-8 3050 were used in the experiments.

3.1.2 Instruments

The spin coater was used for coating of the photoresists on the Si wafer. During the soft lithography process of PDMS microfluidic chip fabrication for photolithography step, the Mask Aligner device was used. While conducting the experiment an Axio Light Microscope, Carl-Zeiss LSM 710 Confocal Microscope (with UV laser and 458, 488, 514, 561, 633 nm laser units) was used for visualization.

3.1.3 Microfluidic Device Design

Microfluidic devices were designed using the AUTOCAD (Autodesk inc.) software. They are displayed in Figure 11.

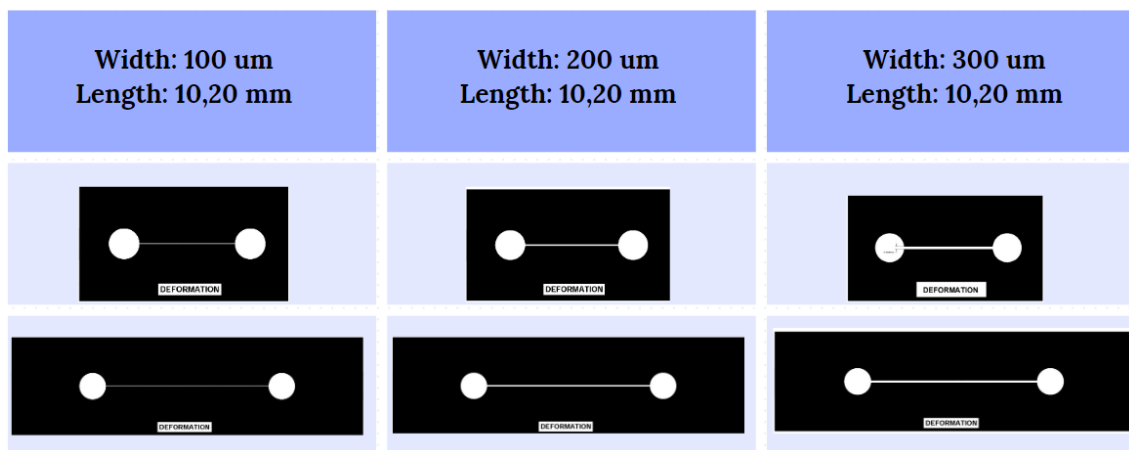


Figure 11: Microfluidic device designs and parameters

3.1.4 PDMS Microchannel Fabrication

In order to form microchannels, SU-8 3050 negative photoresist (Microchem Corp., Westborough, MA, USA) was carefully applied to a one side polished 4-inch silicon wafer (University Wafer, Inc., Boston, MA, USA) at 1000 revolutions per minute (rpm) using a spin coater. Then, using a KLA Tensor profiler, the thickness of the SU-8 3050 resin, which had been evenly placed to the silicon wafer, was determined as 100 μm .

Using an optical lithography mask and Mask Aligner UV-Lithography device (Midas System Co., Ltd., Daejeon, Korea, MDA-60MS Mask Aligner 4"), the photoresist-coated silicon wafer was exposed to UV light. After this, the photoresist was developed using SU-8 developer solution (Microchem Corp.) which formed the required geometries.

After the microfabrication process was completed, SU-8 molds were used to cast PDMS. Prepolymer base and curing base were carefully mixed at a 10:1 ratio for 10 minutes. The mixture was then poured over the SU-8 mold within a plastic petri dish. The PDMS mixture was placed under a vacuum desiccator. The degassed PDMS mixture was then cured for three hours at 75 degrees Celsius in an oven.

The glass-microchannel bonding procedure began when the mold and PDMS microchannels were carefully separated after PDMS had successfully cured. The thin glass slide and PDMS channel were activated by subjecting them to oxygen plasma for one minute within an oxygen plasma generator. Finally, by properly aligning and pressing the matching surfaces, a permanent link was formed, leading to closed microchannel topologies.

At least 2 hours after bonding, leak tests were performed to measure the quality of bonding and production. The working fluid was passed through the channels under a light microscope, and it was visualized whether the liquid leaked between PDMS and glass or not.

3.1.5 Visualization in Microchannel

Imaging was performed under a confocal microscope to detect the deformation of the channels. The confocal microscope provides us with a 3D channel confirmation by taking layer by layer images. Rhodamine B was used to provide fluorescence in the flow to clearly determine the structure of the channel and to facilitate image analysis. First,

images of the channels without flow were taken to be used as a threshold in the subsequent image analysis. Then a syringe pump was employed to deliver the working fluid through the channels at controlled flow rates of 204, 429, 691, and 1000 $\mu\text{L}/\text{min}$. The experiments were repeated for each chip and each flow rate separately. The experimental setup is shown in Figure 12.

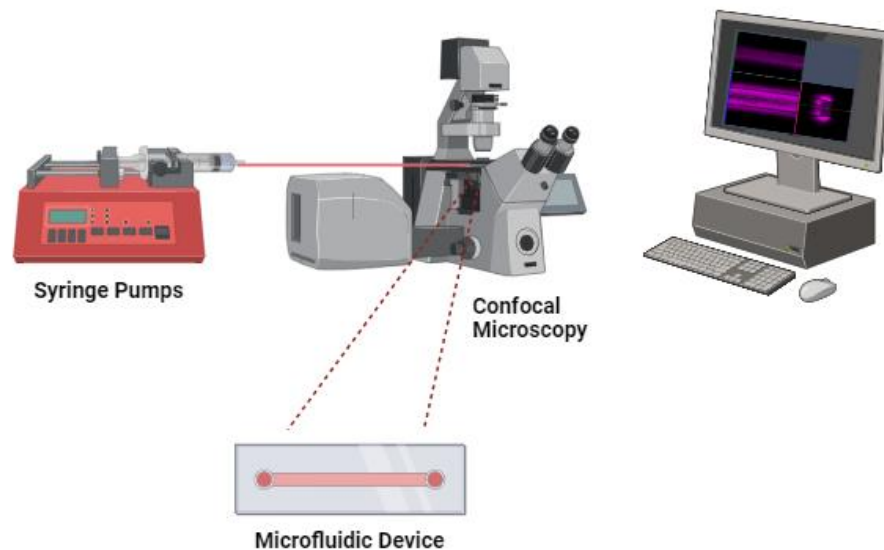


Figure 12: Experimental setup of deformation experiments under confocal microscope.

3.1.6 Image Processing

Microscopy images were analyzed using the ZEN and ImageJ software. Cross sections of images were saved with a scale bar. Then to make boundaries sharpened, threshold was applied on the images. To measure the distance (height) from the bottom of the microchannel to top, a line was drawn (Figure 13). First, the height h_0 of the channel (the point where deformation is zero) was determined for the case of no flow. Then, for images taken at each flow rate, the channel height was analyzed. The difference between these channel heights and h_0 was calculated to find the deformation. The percentage deformation was then calculated as $(h_1-h_0)100/h_0$. This analysis was repeated for five times for each channel and flow rate. The average and error bars were then calculated based on the repeated measurements.

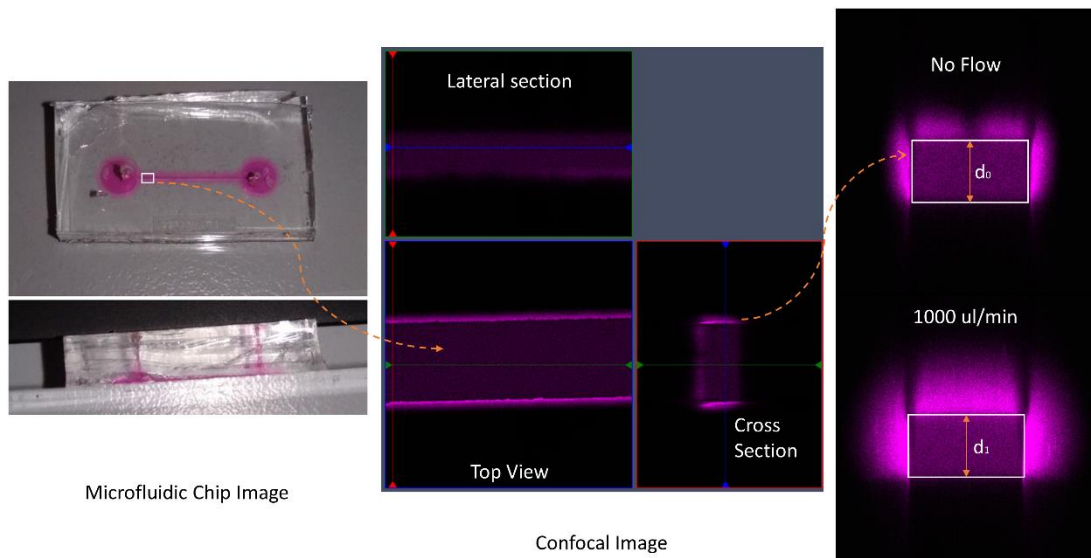


Figure 13: Confocal Images of Microfluidic Device

Images were taken from a channel with dimensions of a length of 10 mm, a width of 100 μm , and a height of 100 μm , at points 0, 1, 2, 3, 4, and 5 mm from the entrance of the channel (Figure 14). Deformation decreases from the entrance to the exit. Therefore, for all other analyses, the deformation at the entrance point of the channel was calculated.

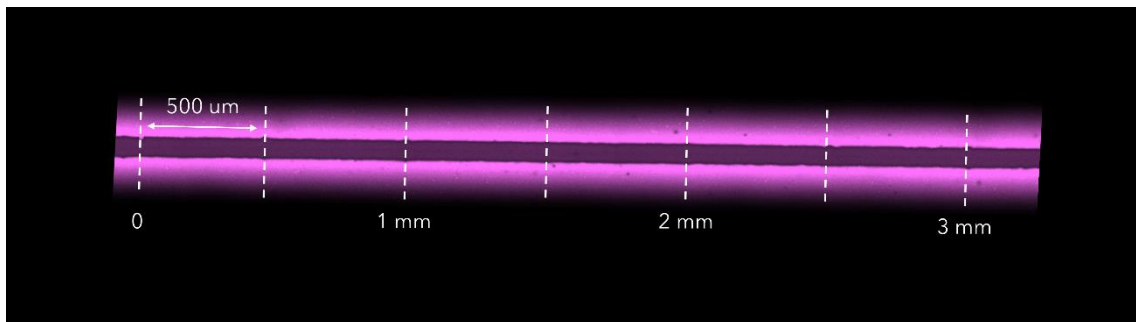


Figure 14: Part of channel with distance distribution for image analysis.

3.2 Result and Discussion

3.2.1 Calculations of Flow Parameters

In order to interpret the flow, some major parameters need to be determined. Reynolds number is an important parameter to determine the flow regime. Small Reynolds number corresponds to laminar flow, while turbulent flow occurs at high Reynolds numbers. In

applications such as separation, mixing and particle focusing, which take advantage of the patriarchal forces of the flow, the characteristic of the flow provide the basis for the successful operation of the microfluidic device.

Reynolds number is expressed as:

$$\mathbf{Re} = \frac{\rho v D_h}{\mu}$$

where D_h is the hydraulic diameter, μ is the fluid viscosity, v is the fluid's characteristic velocity, and ρ is the fluid density. The cross-sectional shape of the channel affects the calculated hydraulic diameter. For $Re < 2000$, the flow is laminar . For large Reynolds number, the flow is regarded as turbulent [21].

The distance required for the flow to become fully developed is represented by the entrance length [22]. For laminar flows, the hydrodynamic entrance length can be calculated as:

$$\mathbf{Le} \approx 0.05 D_h Re$$

where D_h is the hydraulic diameter and is expressed as:

$$\mathbf{D_h} = \frac{4A_c}{P}$$

where A_c is the cross sectional area and P is the perimeter of the cross section of the channel.

Pressure drop is another parameter which can be found as;

$$\Delta p = f \left(\frac{L}{D_h} \right) \frac{(\rho v^2)}{2}$$

where f is the Darcy friction factor (dimensionless), L is the channel length (m), D_h is the hydraulic diameter of the channel (m), ρ is the density of the fluid (kg/m^3), v is the average flow velocity (m/s). The friction factor depends on the channel geometry and Reynolds number. Friction number flows is included for fully developed laminar in Figure 15.

Nusselt number and friction factor for fully developed laminar flow in tubes of various cross sections ($D_h = 4A_c/p$, $Re = V_{avg}D_h/\nu$ and $Nu = hD_h/k$)

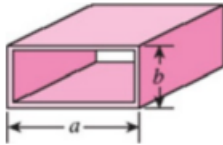
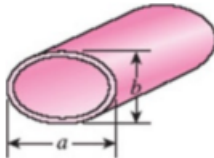
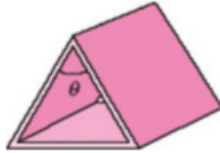
Tube Geometry	a/b or θ°	Nusselt Number		Friction factor f	
		$T_s = \text{Const.}$	$\dot{q}_s = \text{Const.}$		
Circle	—	3.66	4.36	64.00/Re	
Rectangle		1	2.98	3.61	56.92/Re
		2	3.39	4.12	62.20/Re
		3	3.96	4.79	68.36/Re
		4	4.44	5.33	72.92/Re
		6	5.14	6.05	73.80/Re
		3	5.60	6.49	32.32/Re
		∞	7.54	8.24	96.00/Re
Ellipse		1	3.66	4.36	64.00/Re
		2	3.74	4.56	67.28/Re
		4	3.79	4.88	72.96/Re
		8	3.72	5.09	76.60/Re
		16	3.65	5.18	78.16/Re
		Isosceles Triangle		θ	
10°	1.61	2.45		50.80/Re	
30°	2.26	2.91		52.28/Re	
60°	2.47	3.11		53.32/Re	
90°	2.34	2.98		52.60/Re	
	120°	2.00	2.68	50.96/Re	

Figure 15: Nusselt number and friction factors for fully developed laminar flows [23,24].

The calculated pressure drop and Reynolds number values are tabulated in Table 1.

Table 1: Pressure drop and Reynolds number

Chip Dimension	Flow Rate (Q)	Reynolds Number	Pressure Drop (ΔP)
L=10 mm W=100 μ m	204 μ l/min	38.1	8.6 kPa
H= 100 μ m	429 μ l/min	80.2	18.1 kPa
	691 μ l/min	129.1	29.2 kPa
	1000 μ l/min	186.9	42.2 kPa

L=10 mm W=200 um	204 ul/min	25.4	2.6 kPa
H= 100 um	429 ul/min	53.4	5.5 kPa
	691 ul/min	86.1	8.9 kPa
	1000 ul/min	124.6	12.9 kPa
L=10 mm W=300 um	204 ul/min	19.1	1.5 kPa
H= 100 um	429 ul/min	40.1	3.2 kPa
	691 ul/min	64.5	5.2 kPa
	1000 ul/min	93.4	7.7 kPa
L=20 mm W=100 um	204 ul/min	38.1	17.2 kPa
H= 100 um	429 ul/min	80.2	36.2 kPa
	691 ul/min	129.1	58.3 kPa
	1000 ul/min	186.9	92.4 kPa
L=20 mm W=200 um	204 ul/min	25.4	5.3 kPa
H= 100 um	429 ul/min	53.4	11.1 kPa
	691 ul/min	86.1	17.9 kPa
	1000 ul/min	124.6	25.9 kPa
L=20 mm W=300 um	204 ul/min	19.1	3.1 kPa
H= 100 um	429 ul/min	40.1	6.4 kPa
	691 ul/min	64.5	10.4 kPa
	1000 ul/min	93.4	15.0 kPa

3.2.2 Deformation Measurements

Figure 16 shows the results of image analysis using images taken from different locations along the channel length. In these analyses, microfluidic chips with 10 mm length and 100 μm width and 100 μm length were used, and the experiments were performed at flow rates of 204, 429, 691 $\mu\text{l}/\text{min}$. According to Fig 17, there is a decrease in deformation from the channel inlet to the channel outlet. This is due to the change in the pressure of the flow along the channel. Accordingly, the pressure drops from the inlet to the outlet. Similar results (Fig 2.) were obtained in the literature (Gervais et al.) [18].

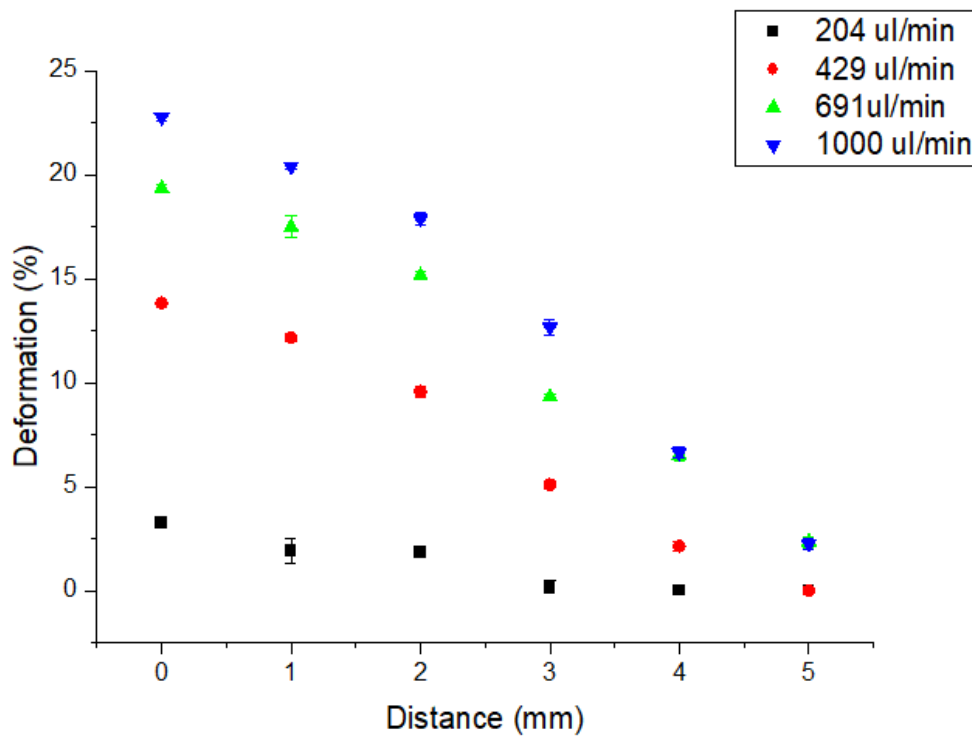


Figure 16: Deformation of PDMS microchannel along the length channel

In Figure 17, deformation profiles of 10 mm length channels with different widths are shown. For a microfluidic chip, as the flow rate increases, the deformation increases correspondingly. However, as the width increases, the deformation is observed to decrease, which is due to the change in pressure drop with width as also shown in Fig. 18.

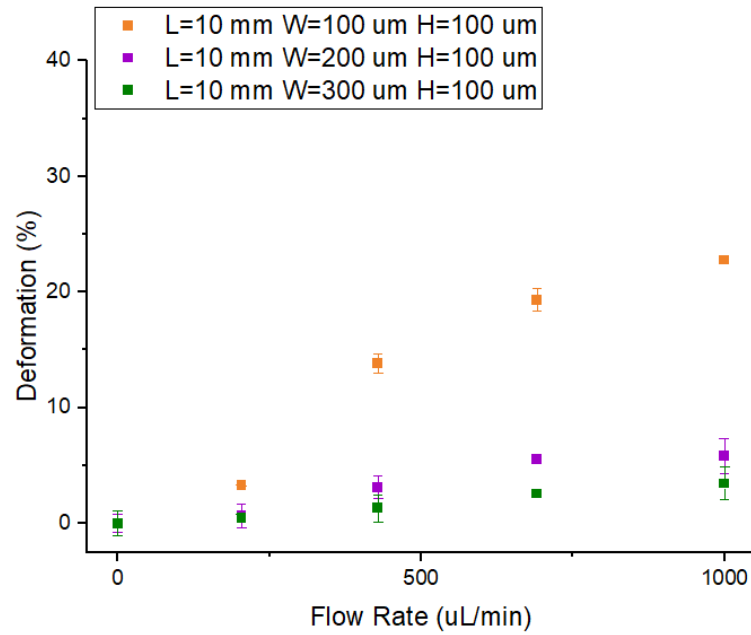


Figure 17: Deformation of microchannels with 10 mm length

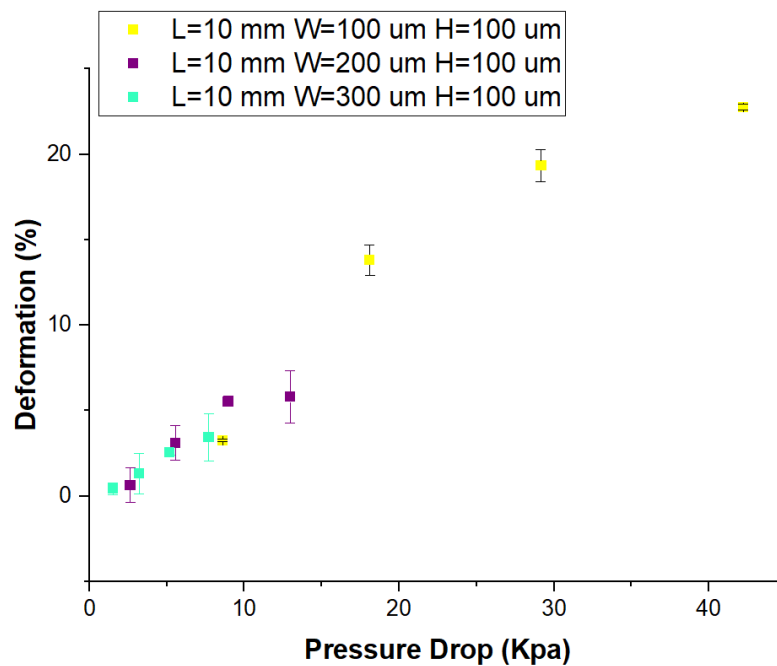


Figure 18: Deformation of microchannels with 10 mm length (in terms of pressure drop).

The deformation rates of the 20 mm long microchannel are shown in Figure 19 and Figure 20. An increase in the deformation can be observed with flow rate. When comparing the deformations of microchannels with lengths of 20 mm and 10 mm, it can be seen that

despite the higher pressure drop in the channel with a length of 20 mm, the maximum deformation values of both channels are close to each other. PDMS microchannels were fabricated under the same conditions, ensuring identical elasticity. The observed deformation is a consequence of the material's elasticity, and the constant profile regarding deformation despite an increase in pressure could suggest that the material has reached its elastic limit. In other words, the maximum deformation ratio of the PDMS microfluidic chips used in the experiments is approximately 25%.

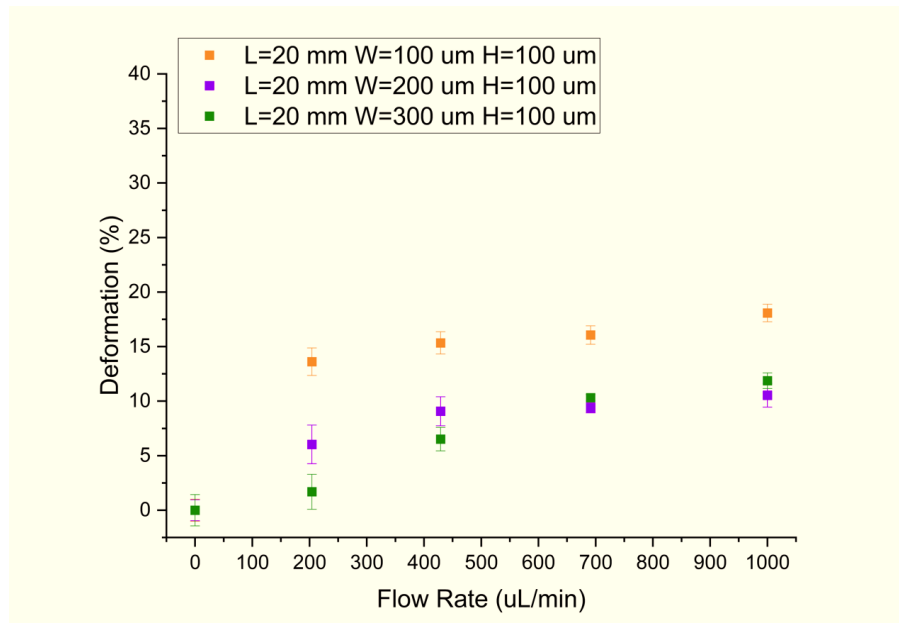


Figure 19: Deformation of microchannels with 20 mm length

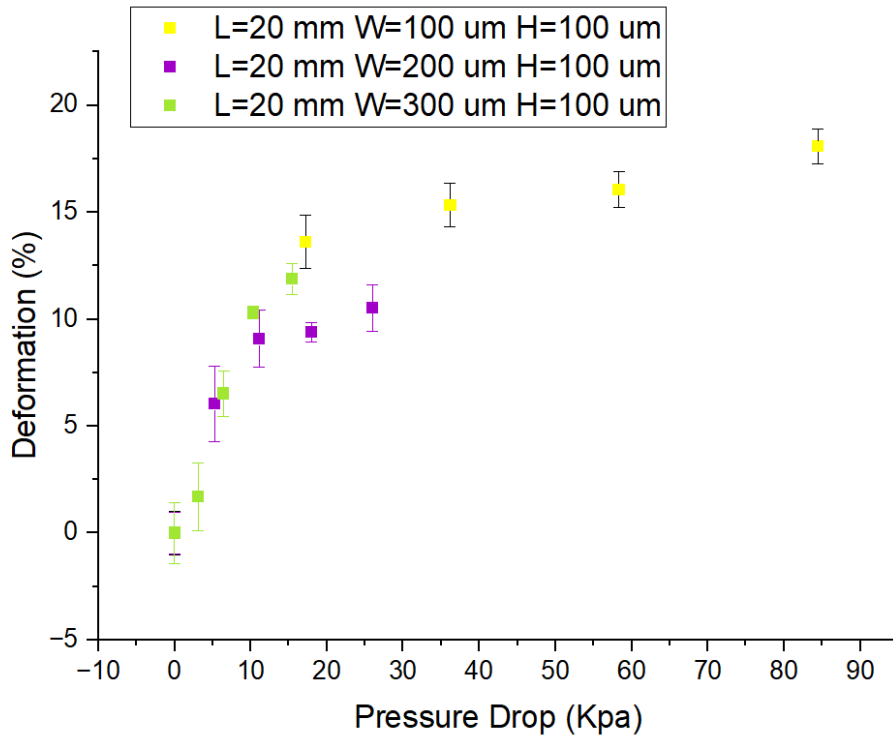


Figure 20: Deformation of microchannels with 20 mm length, (in terms of pressure drop).

Three microchannels with identical dimensions but varying Young's modulus values, which were achieved by altering the curing agent ratio in PDMS fabrication, were employed. Atomic force microscopy (AFM) determined the Young's modulus of each channel (Table 2). Subsequently, image analysis quantified the deformation rate at four flow rates: 204, 429, 691, and 1000 $\mu\text{L}/\text{min}$ (Figure 20).

Table 2: Elasticity of PDMS channels with different curing ratios

Curing Ratio:	1/5	1/10	1/20
Elasticity (Young Modulus):	19.5 kPa	8.1 kPa	2.78 kPa

The results reveal a significant impact of elasticity on deformation, particularly at the lowest flow rate of 204 $\mu\text{L}/\text{min}$. The channels with higher Young's modulus exhibit lower deformation rate which highlights the direct correlation between stiffness and resistance to deformation. This difference diminishes with flow rate, as evident in the converging

deformation curves in Figure 21. These findings suggest that the influence of elasticity on deformation becomes less pronounced at higher pressures.

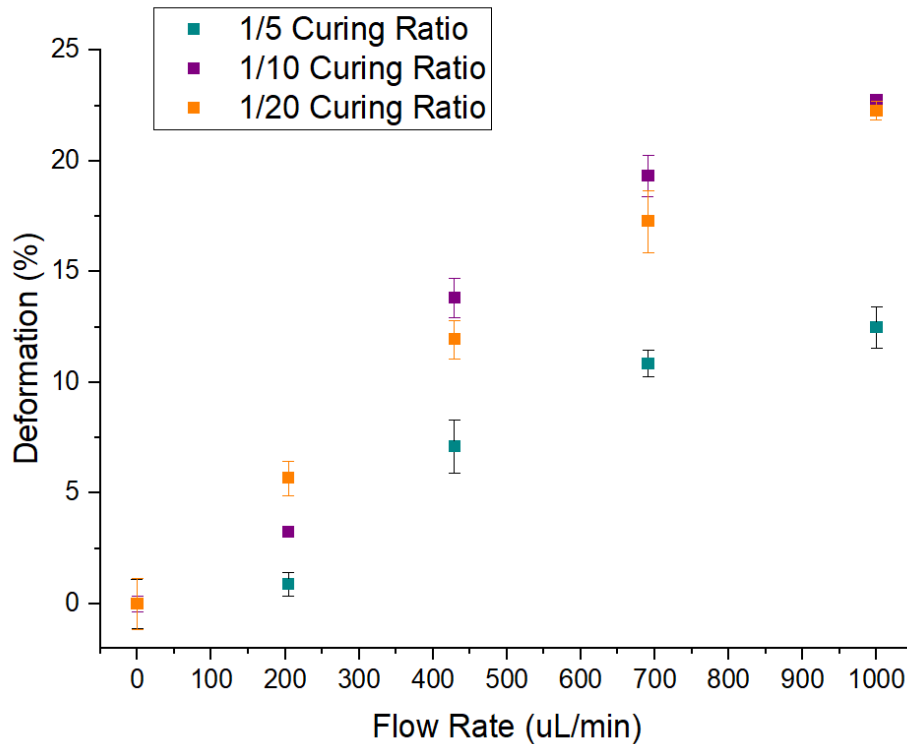


Figure 21: Deformation of microchannels with different elasticity and dimensions of 10 mm length 100 μ m width 100 μ m height.

3.3 Conclusion

This section analyzed and compared the deformations of microfluidic devices with different dimensions and elasticities. Deformations in the channels were identified through the analysis of images obtained with confocal microscopy. The results indicate that the deformation ratio of microchannels with the same dimensions is particularly dependent on elasticity at low flow rates. As the flow rate increases, the influence of elasticity decreases, suggesting that fluid pressure becomes the dominant factor in channel deformation at higher flow regimes. As a future research effort, the deformation effect on a real microfluidic application, such as particle focusing, will be explored. Experiments involving flows with particles will be performed.

CHAPTER 4.

CONCLUSION

This thesis consists of two parts. In the first part, the impact of using different molds on the curing of PDMS was investigated. PDMS was cured at temperatures of 55°C, 65°C, and 75°C for durations of 2, 6, and 12 hours using PLA, PET AL, and resin molds. Subsequently, the mechanical, thermal, and structural properties of these samples were compared. In the first part, it is revealed that the mold type does not affect PDMS curing efficiency however using different mold material affects both mechanical properties of the material and curing kinetics of PDMS.

In the second part, deformations in microfluidic chips with different dimensions and elasticities were analyzed and compared. According to the findings, at low flow rates, the deformation ratio of microchannels with the same dimensions is notably influenced by elasticity. However, as the flow rate rises, the impact of elasticity diminishes.

Both parts of the thesis highlight that variations in fabrication conditions of microscale devices can lead to significant effects on the material and shape. Elasticity is an important feature of PDMS for compatibility with cells in organ-on-a-chip applications. In this thesis it is shown that the used mold material affects the curing of PDMS and material's mechanical properties in addition to the temperature, curing ratio, and curing duration.

FUTURE WORK

As future work, the effects of mold size and shape on curing and elasticity could be investigated using alternative methods such as compression for a more comprehensive comparison. In addition, the impact of PDMS microchannel deformation on particle focusing will be studied using micro-particles to directly assess its effect in a real microfluidic application.

CHAPTER 5. REFERENCES

- [1]: Konku-Asase, Y., Yaya, A., & Kan-Dapaah, K. (2020). Curing Temperature Effects on the Tensile Properties and Hardness of γ -Fe₂O₃ Reinforced PDMS Nanocomposites. *Advances in Materials Science and Engineering*, 2020. <https://doi.org/10.1155/2020/6562373>
- [2]: Gervais, T., El-Ali, J., Günther, A., & Jensen, K. F. (2006). Flow-induced deformation of shallow microfluidic channels. *Lab on a Chip*, 6(4). <https://doi.org/10.1039/b513524a>
- [3]: Pérez, J. F., Llanos, J., Sáez, C., López, C., Cañizares, P., & Rodrigo, M. A. (2018). Development of an innovative approach for low-impact wastewater treatment: A microfluidic flow-through electrochemical reactor. *Chemical Engineering Journal*, 351. <https://doi.org/10.1016/j.cej.2018.06.150>
- [4]: Cong, H., & Pan, T. (2008). Photopatternable conductive PDMS materials for microfabrication. *Advanced Functional Materials*, 18(13). <https://doi.org/10.1002/adfm.200701437>
- [5]: Bardelli, T., Marano, C., & Briatico Vangosa, F. (2021). Polydimethylsiloxane crosslinking kinetics: A systematic study on SYLGARD184 comparing rheological and thermal approaches. *Journal of Applied Polymer Science*, 138(39). doi:10.1002/app.51013
- [6]: Johnston, I. D., McCluskey, D. K., Tan, C. K. L., & Tracey, M. C. (2014). Mechanical characterization of bulk Sylgard 184 for microfluidics and microengineering. *Journal of Micromechanics and Microengineering*, 24(3). <https://doi.org/10.1088/0960-1317/24/3/035017>
- [7]: Torino, S., Corrado, B., Iodice, M., & Coppola, G. (2018). Pdms-based microfluidic devices for cell culture. In *Inventions* (Vol. 3, Issue 3). <https://doi.org/10.3390/inventions3030065>
- [8]: Zhao, Y., Demirci, U., Chen, Y., & Chen, P. (2020). Multiscale brain research on a microfluidic chip. In *Lab on a Chip* (Vol. 20, Issue 9). <https://doi.org/10.1039/c9lc01010f>
- [9]: Kim, J. H., Sim, J., & Kim, H. J. (2018). Neural stem cell differentiation using microfluidic device-generated growth factor gradient. *Biomolecules and Therapeutics*, 26(4). <https://doi.org/10.4062/biomolther.2018.001>
- [10]: Jeon, J. S., Bersini, S., Whisler, J. A., Chen, M. B., Dubini, G., Charest, J. L., Moretti, M., & Kamm, R. D. (2014). Generation of 3D functional microvascular networks with human mesenchymal stem cells in microfluidic systems. *Integrative Biology (United Kingdom)*, 6(5). <https://doi.org/10.1039/c3ib40267c>
- [11]: Islam, M. S., & Chen, X. (2023). Continuous CTC separation through a DEP-based contraction–expansion inertial microfluidic channel. *Biotechnology Progress*, 39(4). <https://doi.org/10.1002/btpr.3341>

- [12]: Sajeesh, P., & Sen, A. K. (2014). Particle separation and sorting in microfluidic devices: A review. In *Microfluidics and Nanofluidics* (Vol. 17, Issue 1). <https://doi.org/10.1007/s10404-013-1291-9>
- [13]: Glasgow, I., & Aubry, N. (2003). Enhancement of microfluidic mixing using time pulsing. *Lab on a Chip*, 3(2). <https://doi.org/10.1039/b302569a>
- [14]: Introduction to Tensile Testing. (2022). In *Tensile Testing*. <https://doi.org/10.31399/asm.tb.tt2.t51060001>
- [15]: Fischer-Cripps, A. C. (2004). *Analysis of Nanoindentation Test Data*. https://doi.org/10.1007/978-1-4757-5943-3_3
- [16]: Suriano, R., Credi, C., Levi, M., & Turri, S. (2014). AFM nanoscale indentation in air of polymeric and hybrid materials with highly different stiffness. *Applied Surface Science*, 311. <https://doi.org/10.1016/j.apsusc.2014.05.108>
- [17]: Vekstein, G. (2020). - Theory of elasticity. In *Physics of Continuous Media*. <https://doi.org/10.1201/b16095-7>
- [18]: Gervais, T., El-Ali, J., Günther, A., & Jensen, K. F. (2006). Flow-induced deformation of shallow microfluidic channels. *Lab on a Chip*, 6(4). <https://doi.org/10.1039/b513524a>
- [19]: Lee, J. N., Park, C., & Whitesides, G. M. (2003). Solvent Compatibility of Poly(dimethylsiloxane)-Based Microfluidic Devices. *Analytical Chemistry*, 75(23). <https://doi.org/10.1021/ac0346712>
- [20]: Razavi Bazaz, S., Kashaninejad, N., Azadi, S., Patel, K., Asadnia, M., Jin, D., & Ebrahimi Warkiani, M. (2019). Rapid Softlithography Using 3D-Printed Molds. *Advanced Materials Technologies*, 4(10). <https://doi.org/10.1002/admt.201900425>
- [21]: Beebe, D. J., Mensing, G. A., & Walker, G. M. (2002). Physics and applications of microfluidics in biology. In *Annual Review of Biomedical Engineering* (Vol. 4). <https://doi.org/10.1146/annurev.bioeng.4.112601.125916>
- [22]: Kutter, J. P., & Klank, H. (2003). Microfluidics – Theoretical Aspects. In *Microsystem Engineering of Lab-on-a-Chip Devices*. <https://doi.org/10.1002/3527601651.ch3>
- [23]: Zohuri, B. (2017). Laminar incompressible forced convection. *Thermal-Hydraulic Analysis of Nuclear Reactors*, 147–221. doi:10.1007/978-3-319-53829-7_5
- [24]: Morihara, H., & Ta-Shun Cheng, R. (1973). Numerical solution of the viscous flow in the entrance region of parallel plates. *Journal of Computational Physics*, 11(4), 550–572. doi:10.1016/0021-9991(73)90137-x

- [25]: Tranchida, D., Piccarolo, S., & Soliman, M. (2006). Nanoscale mechanical characterization of polymers by AFM nanoindentations: Critical approach to the elastic characterization. *Macromolecules*, 39(13). <https://doi.org/10.1021/ma052727j>
- [26]: Fujii, T. (2002). PDMS-based microfluidic devices for biomedical applications. *Microelectronic Engineering*, 61–62. [https://doi.org/10.1016/S0167-9317\(02\)00494-X](https://doi.org/10.1016/S0167-9317(02)00494-X)
- [27]: Raj M, K., & Chakraborty, S. (2020). PDMS microfluidics: A mini review. In *Journal of Applied Polymer Science* (Vol. 137, Issue 27). <https://doi.org/10.1002/app.48958>
- [28]: Raninga, R., Page, K., & Parkin, I. P. (2014). Polydimethylsiloxane coated glass frits for low-cost and reusable water-organic solvent separation. *Chemical Communications*, 50(84). <https://doi.org/10.1039/c4cc05663a>
- [29]: Gervais, T., El-Ali, J., Günther, A., & Jensen, K. F. (2006). Flow-induced deformation of shallow microfluidic channels. *Lab on a Chip*, 6(4). <https://doi.org/10.1039/b513524a>
- [30]: Pérez, J. F., Llanos, J., Sáez, C., López, C., Cañizares, P., & Rodrigo, M. A. (2018). Development of an innovative approach for low-impact wastewater treatment: A microfluidic flow-through electrochemical reactor. *Chemical Engineering Journal*, 351. <https://doi.org/10.1016/j.cej.2018.06.150>
- [31]: Verma, M. K. S., Majumder, A., & Ghatak, A. (2006). Embedded template-assisted fabrication of complex microchannels in PDMS and design of a microfluidic adhesive. *Langmuir*, 22(24). <https://doi.org/10.1021/la062516n>
- [32]: Jeon, H., Kwon, T., Yoon, J., & Han, J. (2022). Engineering a deformation-free plastic spiral inertial microfluidic system for CHO cell clarification in biomanufacturing. *Lab on a Chip*, 22(2). <https://doi.org/10.1039/d1lc00995h>
- [33]: Mehboudi, A., & Yeom, J. (2019). Experimental and theoretical investigation of a low-Reynolds-number flow through deformable shallow microchannels with ultra-low height-to-width aspect ratios. *Microfluidics and Nanofluidics*, 23(5). <https://doi.org/10.1007/s10404-019-2235-9>
- [34]: Ng, P. F., Lee, K. I., Yang, M., & Fei, B. (2019). Fabrication of 3D PDMS microchannels of adjustable cross-sections via versatile gel templates. *Polymers*, 11(1). <https://doi.org/10.3390/polym11010064>
- [35]: Sugiura, Y., Hiram, H., & Torii, T. (2015). Fabrication of microfluidic valves using a hydrogel molding method. *Scientific Reports*, 5. <https://doi.org/10.1038/srep13375>

- [36]: Hunter, L., Gala de Pablo, J., Stammers, A. C., Thomson, N. H., Evans, S. D., & Shim, J. uk. (2020). On-chip pressure measurements and channel deformation after oil absorption. *SN Applied Sciences*, 2(9). <https://doi.org/10.1007/s42452-020-03288-8>
- [38]: Lin, I. K., Liao, Y. M., Liu, Y., Ou, K. S., Chen, K. S., & Zhang, X. (2008). Viscoelastic mechanical behavior of soft microcantilever-based force sensors. *Applied Physics Letters*, 93(25). <https://doi.org/10.1063/1.3056114>
- [39]: Onal, S., Alkaisi, M. M., & Nock, V. (2021). A Flexible Microdevice for Mechanical Cell Stimulation and Compression in Microfluidic Settings. *Frontiers in Physics*, 9. <https://doi.org/10.3389/fphy.2021.654918>
- [40]: Thangawng, A. L., Ruoff, R. S., Swartz, M. A., & Glucksberg, M. R. (2007). An ultra-thin PDMS membrane as a bio/micro-nano interface: Fabrication and characterization. *Biomedical Microdevices*, 9(4). <https://doi.org/10.1007/s10544-007-9070-6>
- [41]: Qu, J., Zhang, W., Jung, A., Silva-Da Cruz, S., & Liu, X. (2017). Microscale Compression and Shear Testing of Soft Materials Using an MEMS Microgripper with Two-Axis Actuators and Force Sensors. *IEEE Transactions on Automation Science and Engineering*, 14(2). <https://doi.org/10.1109/TASE.2016.2613684>
- [42]: Lin, I. K., Liao, Y. M., Liu, Y., Chen, K. S., & Zhang, X. (2008). Elastic and viscoelastic characterization of polydimethylsiloxane (PDMS) for cell-mechanics applications. *Materials Research Society Symposium Proceedings*, 1052. <https://doi.org/10.1557/proc-1052-dd03-02>
- [43]: Zhang, X., Chu, H. K., Zhang, Y., Bai, G., Wang, K., Tan, Q., & Sun, D. (2015). Rapid characterization of the biomechanical properties of drug-treated cells in a microfluidic device. *Journal of Micromechanics and Microengineering*, 25(10). <https://doi.org/10.1088/0960-1317/25/10/105004>
- [44]: de Almeida Monteiro Melo Ferraz, M., Nagashima, J. B., Venzac, B., le Gac, S., & Songsasen, N. (2020). 3D printed mold leachates in PDMS microfluidic devices. *Scientific Reports*, 10(1). <https://doi.org/10.1038/s41598-020-57816-y>
- [45]: Sun, M., Xie, Y., Zhu, J., Li, J., & Eijkel, J. C. T. (2017). Improving the Resolution of 3D-Printed Molds for Microfluidics by Iterative Casting-Shrinkage Cycles. *Analytical Chemistry*, 89(4). <https://doi.org/10.1021/acs.analchem.6b05148>